

Article 301

Spin Structures and Spin Wave Excitations

I. A. Zaliznyak

1. Introduction and Outline

Technological progress of recent years clearly brings to the forefront the ever-increasing importance of magnetism and magnetic materials in the everyday life. Detailed understanding of microscopic atomic structure and origins of magnetic phenomena now appears as key to further advances in diverse fields of science and technology. Although studies of magnetic structures and excitations form rapidly expanding area of modern science offering new discoveries and surprises without an end in sight, large body of experimental material and theoretical work accumulated over the past half a century can be understood in the framework of a simple microscopic description based on semi-classical treatment of systems of localized spins of magnetic ions. This article presents a brief survey of common types of spin structures and excitations found in magnetic crystals that can be described in the framework of such semi-classical spin-wave approach. Experimental examples of neutron scattering studies, as best known to the author, are presented for each type, and discussed in the context of an up-to-date presentation of the linear spin-wave theory, perhaps, at the undergraduate level.

The article is organized as follows. Introductory second section outlines fundamental connection between magnetism and electronic spins from which it arises, spin interactions that are at the origin of cooperative magnetic phenomena are discussed in the third section, the fourth and the fifth sections present survey of different spin structures and spin-wave excitations, respectively, and the last section gives a brief summary.

2. Magnetism and Spin

Magnetism of many-electron condensed matter systems is a cooperative macroscopic quantum phenomenon originating from the fundamental relationship between the magnetic moment \mathbf{M} and the angular momentum \mathbf{J} ,

$$\mathbf{M} = \gamma \mathbf{J}, \quad (1)$$

where γ is the so-called gyromagnetic ratio [1,2]. This expression is a counterpart of the famous equivalence relation between magnetic field \mathbf{H} and rotation with angular velocity

$$\boldsymbol{\Omega}_L = \frac{|e|\hbar}{2m_e c} \mathbf{H} \text{ known as Larmor's theorem, } e \text{ and } m_e \text{ are electron's charge and mass and}$$

c is the velocity of light in vacuum. If a system interacts with an anisotropic environment, such as an atom in crystal's electric field, \mathbf{M} and \mathbf{J} might be not co-aligned and the gyromagnetic ratio becomes a tensor quantity, $\gamma_{\alpha\beta}$.

Magnetic moment associated with the Ampere's molecular electric current produced by an electron moving on an atomic orbit can already be derived semi-classically from the Biot-Savart law,

$$\boldsymbol{\mu}_e = -\frac{\mu_B}{\hbar} [\mathbf{r}_e \times \mathbf{p}_e] = -\frac{\mu_B}{\hbar} \mathbf{l}_e = -\frac{|e|\hbar}{2m_e c} \mathbf{l}_e. \quad (2)$$

This establishes the gyromagnetic ratio for the orbital motion, $\gamma_l = -\frac{|e|\hbar}{2m_e c}$. This ratio is negative, so electron's orbital magnetic moment is opposite to its orbital angular momentum. The magnetism of moving electric charges, however, is grossly insufficient for explaining magnetic properties of matter, such as e.g. magnetism of the lodestone (magnetite) known since ancient times, which is why it was one of the longest-standing problems in the history of science [3]. Magnetic fields produced by orbital Ampere currents, like artificial magnetic fields from electromagnets, are of electro-dynamic origin. They are caused by non-relativistic motion of electric charges and therefore contain a relativistically small factor, $\sim \alpha \approx 1/137$. The energy of magnetic interaction between two magnetic dipoles associated with Ampere orbital currents of two electrons at a distance $r = 1 \text{ \AA}$, each carrying 1 Bohr magneton, $\mu_B = |e|\hbar/(2m_e c) = 0.927 \cdot 10^{-20} \text{ erg/Gs}$,

$$V(\mathbf{r}) = -\left\{ \frac{8\pi}{3} (\boldsymbol{\mu}_1 \cdot \boldsymbol{\mu}_2) \delta(\mathbf{r}) - \frac{(\boldsymbol{\mu}_1 \cdot \boldsymbol{\mu}_2)}{r^3} + \frac{3(\boldsymbol{\mu}_1 \cdot \mathbf{r})(\boldsymbol{\mu}_2 \cdot \mathbf{r})}{r^5} \right\}, \quad (3)$$

is only $\sim \mu_B^2 / (k_B r^3) \approx 0.6 \text{ Kelvin}$. This is way too small compared with the entropy contribution to the free energy to explain the existence of magnetism at room temperature and above. In addition, a simple theorem, established independently by N. Bohr and J. H. van Leeuwen, in fact prohibits magnetism in a system of classical electrons in thermal equilibrium [3].

Therefore, room-temperature magnetism fundamentally could not be described by classical electrodymanics and was only explained with the devise of quantum mechanics in the early 20th century. It is a consequence of the existence of an additional quantum degree of freedom of an electron, its spin [4,5]. In quantum mechanics electron at rest

still possesses a quantum of “internal” angular momentum, $\hbar s_e$ (\hbar is the Planck’s constant), described by the spin angular momentum operator \mathbf{s}_e of magnitude $s_e = 1/2$,

$$\mathbf{s}_e^2 = s_e(s_e + 1) = \frac{3}{4}, \quad [s_e^x, s_e^y] = i s_e^z, \quad \text{etc.} \quad (4)$$

There is also a magnetic moment of magnitude $\mu_{se} = \mu_B \left(1 + \frac{\alpha}{2\pi} - \dots\right) \approx 1.001\mu_B$ associated with electron’s spin [6]. It is aligned opposite to spin angular momentum,

$$\boldsymbol{\mu}_{se} = -g_s \mu_B \mathbf{s}_e = \gamma_s \cdot (\frac{1}{2} \hbar \mathbf{s}_e), \quad \gamma_s = -g_s \frac{|e| \hbar}{2m_e c}, \quad (5)$$

where $g_s \approx 2.002$ is Lande g-factor and γ_s is spin gyromagnetic ratio for the free electron which, like γ_l , is also negative. Neglecting a $\approx 0.1\%$ relativistic correction, $\gamma_s = 2\gamma_l$. In addition to the orbital angular momentum \mathbf{L} , magnetic moment of a many-electron atom is determined by its total spin,

$$\mathbf{S} = \sum_e \mathbf{s}_e, \quad (6)$$

where the summation can be restricted only to 2S unpaired electrons. Magnetism of condensed matter systems is usually described in terms of interactions between these atomic spins and resulting spin structures and excitations. Within the spin-S ground state multiplet of a Hund’s atom, electronic spins in the incomplete shell can be expressed as

$$\mathbf{s}_e = \pm \frac{1}{2S} \mathbf{S}, \quad \text{with plus sign for the majority and minus for the minority electrons.}$$

For an atomic system with total angular momentum $\mathbf{J} = \mathbf{L} + \mathbf{S}$, atomic gyromagnetic ratio in Eq. (1) is a combination of γ_s and γ_l and in many cases can be calculated using simple

Lande-type formulae [6]. Larmor's equivalence between magnetic field and rotation can be seen in that additional term in the free energy resulting from magnetic field \mathbf{H} and the term arising from Larmor rotation with frequency $\boldsymbol{\Omega}_L = \gamma \cdot \mathbf{H}$ are exactly equal,

$$F_M = -\mathbf{M} \cdot \mathbf{H} = -\gamma \mathbf{J} \cdot \frac{\boldsymbol{\Omega}_L}{\gamma} = -\mathbf{J} \cdot \boldsymbol{\Omega}_L, \quad (7)$$

and can be interchanged as a matter of convenience. This fundamental equivalence immediately leads to the Lagrangian of spin rotations,

$$L = \frac{1}{2} \chi \left(\frac{\boldsymbol{\Omega}}{\gamma} - \mathbf{H} \right)^2, \quad (8)$$

which is at the origin of the powerful macroscopic description of long-wavelength, low-energy excitations in magnetic systems with finite magnetic susceptibility χ and in the presence of magnetic field, in the framework of spin hydrodynamics [7].

3. Spin Interactions and Spin Hamiltonian

Strong interaction between electronic spins leading to magnetism in condensed matter results from a combination of the electrostatic Coulomb repulsion between electrons and a quantum-mechanical coupling between electron spin and co-ordinate wave functions established by Pauli principle which prohibits electrons with the same orbital wave function from also having parallel spins. Hence, a many-electron wave function minimizing the Coulomb energy corresponds to a particular mutual spin alignment of interacting electrons. As was first established by Heisenberg and Dirac, [8,9] within the

first-order approximation of the perturbation theory the electrostatic Coulomb interaction in the many-electron system can be expressed in the form of a spin Hamiltonian,

$$H = \sum_{e,e'} J_{ee'} \left(\mathbf{s}_e \cdot \mathbf{s}_{e'} + \frac{1}{4} \right), \quad (9)$$

which became known as Heisenberg exchange interaction. Expression in brackets, up to a sign, is just a permutation operator for two electrons, tagged e and e' , expressed through their spins. The strength of such direct exchange interaction between two electrons occupying orbital states with wave functions ψ_1 and ψ_2 is given by the overlap integral,

$$J_{ee'} = - \int \psi_1^*(\mathbf{r}_e) \psi_2^*(\mathbf{r}_{e'}) \frac{e^2}{r_{ee'}} \psi_1(\mathbf{r}_{e'}) \psi_2(\mathbf{r}_e) d^3\mathbf{r}_e d^3\mathbf{r}_{e'}, \quad (10)$$

which measures the frequency with which two electrons exchange their orbital states [10]. For the localized orthogonal orbitals the integral is always positive [10,11] and the direct exchange coupling is negative, $J_{ee'} < 0$, favoring parallel, ferromagnetic alignment of electronic spins. This type of interaction is at the origin of the Hund's rule requiring that electrons in an unfilled atomic shell maximize their total spin, and is also involved in the ferromagnetism of 3d metals (Fe, Ni, Co) and other materials. In very few cases, though, straightforward direct exchange is the leading cause of ferromagnetism. In fact, contribution of electron-nuclei Coulomb interaction to the direct electron exchange coupling between two atoms can actually make this coupling positive (e. g. when electron's wave functions have large overlap close to the nuclei), favoring antiparallel, antiferromagnetic spin alignment [12].

In addition to direct exchange, there are a number of indirect exchange mechanisms contributing to coupling between atomic spins in condensed matter systems. The leading cause of the antiferromagnetism in magnetic insulators is the superexchange interaction resulting from the hybridization of wave functions of magnetic 3d ions with those of the intervening non-magnetic anions, [13,14]. In the second-order perturbation theory, virtual electron hopping between the anion and the cation orbitals lowers the energy of the localized electrons. Depending on the electronic and orbital configuration and the resulting hopping matrix elements, direct exchange on the anion site may either lead to antiferromagnetic, or ferromagnetic superexchange [15]. While in insulators with localized electrons superexchange interaction is short-range, typically acting only between the nearest cations bonded by an anion, in semiconductors where anion states form band superexchange interaction can be long-range, extending to distant neighbors [16]. In addition to superexchange, electron hopping through anion site between 3d cations with two degenerate states, such as in $\text{Mn}^{3+}/\text{Mn}^{4+}$ mixed valence systems, can facilitate ferromagnetic coupling, which is known as double exchange [17]. Finally, in metals direct exchange between the localized 3d electrons and itinerant conduction electrons leads to a long-range indirect RKKY interaction whose sign depends on the distance between 3d sites and on the density of delocalized itinerant electrons [18,19]. In view of the fact that spin of each unpaired electron of a Hund's atom is (within the ground-state multiplet) proportional to the total spin \mathbf{S} , in most cases spin Hamiltonian of a system of magnetic atoms in a crystal can, to a good approximation, be written as,

$$\mathbf{H} = \sum_{j \neq j'} J_{jj'} \mathbf{S}_j \cdot \mathbf{S}_{j'} + \sum_j D (S_j^z)^2 - \sum_{j,\beta} \gamma_\beta H_\beta S_j^\beta \equiv \mathbf{H}_E + \mathbf{H}_A + \mathbf{H}_Z. \quad (11)$$

The first term here is the Heisenberg exchange including all direct and indirect exchange interactions, the second term describes the simplest, second-order uniaxial spin anisotropy resulting from electron interaction with the crystal electric field, $\sim \lambda(L^z)^2$, and mediated by the relativistic spin-orbit coupling, $\sim \lambda(\mathbf{L}\mathbf{S})$, and the third term is Zeeman energy in magnetic field \mathbf{H} . The sum is over all atoms tagged by an index j .

While isotropic Heisenberg exchange does select the mutual spin alignment in the ground state spin structure, it has a full $O(3)$ spherical symmetry with respect to spin rotations and therefore does not establish any particular spin orientation with respect to positions of atoms (on the lattice) in the co-ordinate space. Continuum of ground state spin configurations that are related by simultaneous rotation of all spins is allowed. Symmetry of the order parameter in the exchange structure can be understood by moving every spin to a single point without changing its direction. As a result, there might be just one spin group with coinciding spin directions as in the ferromagnet, two groups corresponding to two sublattices with opposite spins, this occurs in antiferromagnets and ferrimagnets, a star of n groups of similar spins with C_n rotational symmetry corresponding to n sublattices in a commensurate spiral magnet, a circle (or ellipse) filled with continuum of spin directions, such as in the incommensurate spin spiral, *etc.*, *cf.* Figure 4 and Figure 5. A complete classification of exchange spin structures was given in Ref. [35].

Anisotropic interactions sensitive to spin direction with respect to atomic positions arise from several sources. First and perhaps most important is the electron spin interaction with crystal electric field mediated by spin-orbit coupling which was mentioned above. Although spin-orbit interaction is a relativistic, electrodynamic effect, it is an intra-atomic interaction and is only small on an atomic energy scale. With $\lambda \sim 100 \text{ K} - 1000 \text{ K}$

and more, it is still very significant on the energy scale of condensed matter systems. Crystal field effects are most pronounced in rare earths and in systems where atom's orbital moment is un-quenched and contributes significantly to the atomic magnetization. In rare earths strong spin-orbit coupling leads to the fine structure of atomic multiplets where total angular momentum \mathbf{J} is a good quantum number and magnetism exists in the ground-state \mathbf{J} multiplet. In most cases, magnetic moment of an atom can still be described by an effective spin and using Eq. (1), perhaps with anisotropic gyromagnetic tensor $\gamma_{\alpha\beta}$. Anisotropic spin interaction with crystal electric field on the same site can be described by a single-ion spin Hamiltonian, which is usually expressed in terms of Stevens operators $O_l^m(\mathbf{S})$ [6,21],

$$H_A = \sum_{l \leq S} \sum_{m=0}^{2l} B_{2l}^m O_{2l}^m(\mathbf{S}), \quad (12)$$

of which only $O_2^0(\mathbf{S}) = 3(S^z)^2 - S(S+1)$ was included in Eq. (11). B_{2l}^m are the crystal field parameters, which, in principle, can be obtained from an *ab initio* calculation of charge distribution in the crystal. These parameters determine spin orientations with respect to the crystal axes and magnetic field. In the absence of magnetic field and for the uniaxial anisotropy of Eq. (11), spins can minimize their energy by aligning parallel to z-axis when anisotropy constant is negative, $D < 0$, (easy axis anisotropy) and by being perpendicular to z-axis when D is positive (easy plane anisotropy).

Electron hopping (i. e. the orbital hybridization) between cation and surrounding anions can lead to a transferred spin anisotropy, which is determined by the electric field at the anion site. In addition, account for spin-orbit interaction may add anisotropic part to the

exchange interaction, resulting in two-spin anisotropy, $H_A = \sum_{\alpha,\beta} D_{jj'}^{\alpha\beta} S_j^\alpha S_{j'}^\beta$, $\alpha, \beta = x, y,$

z. Another small source of anisotropic two-spin coupling is magnetic dipole interaction, Eq. (3). The structure of the diagonal part of anisotropic exchange is similar to Eq. (3) and is often called pseudo-dipole interaction. The off-diagonal part is the antisymmetric exchange of Dzyaloshinsky-Moriya [22,23] and is usually written in the form,

$$H_{DM} = \mathbf{D}_{jj'} \cdot [\mathbf{S}_j \times \mathbf{S}_{j'}]. \quad (13)$$

This interaction is at the origin of weak ferromagnetism of antiferromagnets, Figure 2 (b), and incommensurate spiral spin structures such as shown in Figure 4. Expression for vector \mathbf{D} can be derived in the perturbation theory and depends on matrix elements of the orbital momentum of the interacting atoms. Its direction in the crystal can often be determined from the symmetry of atomic orbitals with respect to the line segment connecting spins j and j' . If there is inversion symmetry with respect to the center of this bond, \mathbf{D} vanishes. For $S=1/2$ ions such as Cu^{2+} , single-ion spin Hamiltonian resulting from the crystal field is just a constant and only two-ion spin anisotropy is possible. In metals and systems with itinerant electrons, the anisotropy of indirect exchange mediated by these electrons can arise not only from their spin-orbital coupling to the crystal field, but also from the spin and wave vector dependent electron scattering due to Fermi surface anomalies, which is sensitive to the spin polarization of electron bands.

4. Spin Structures

While spin Hamiltonian of Eq. (11) is clearly oversimplified, e. g. it assumes localized spins and only includes uniaxial single-ion spin anisotropy, it properly describes great

variety of important cases, some of which are discussed below. It also appears that with some notable exceptions, such as often found in one-dimensional (1D) and two-dimensional (2D) and/or frustrated spin systems where ground state is disordered [24,25,26], spin structures and excitations of this Hamiltonian can be correctly predicted by adopting a semiclassical description based on $1/S$ expansion. This approach, which is justified for large spins, is known as spin wave theory [27,28].

The starting point for spin wave calculation is finding the ground state (GS) spin configuration that has the lowest energy, E_{GS} , for classical spins, i. e. treating spin operators in Eq. (11) as classical vector variables. This neglects all fluctuations and is essentially a mean field approximation. For a system of N identical spins S on a Bravais crystal lattice and without anisotropy and magnetic field ($D = H = 0$), general solution for the classical ground state of Eq. (11) is a co-planar spin spiral [29,30,31],

$$\mathbf{S}_j = \mathbf{S}_Q e^{i\mathbf{Q}\cdot\mathbf{r}_j} + \mathbf{S}_Q^* e^{-i\mathbf{Q}\cdot\mathbf{r}_j}. \quad (14)$$

Ground state spin configuration is thus specified by the order parameter \mathbf{S}_Q , which is simply a Fourier transform of spin structure. This includes ferromagnetic ($\mathbf{Q} = 0$ and all spins are parallel) and antiferromagnetic (there are two spin positions in the lattice, with $\mathbf{Q}\cdot\mathbf{r}_j = 0$ and $\mathbf{Q}\cdot\mathbf{r}_j = \pi$, i. e. there are two sublattices with antiparallel spins) collinear spin structures, cf. Figure 1. In a collinear structure \mathbf{S}_Q in (14) is a real vector of length $S/2$. In a non-collinear spiral spin structure, \mathbf{S}_Q is a complex vector satisfying conditions $\mathbf{S}_Q^2 = 0$ and $2(\mathbf{S}_Q \cdot \mathbf{S}_Q^*) = S^2$ which ensure that all spins have equal length S .

Consequently, its real and imaginary parts are two mutually perpendicular vectors of length $S/\sqrt{2}$. They define the plane to which all spins are confined. Spins follow circularly

polarized rotation in this plane, propagating in the direction of wave vector \mathbf{Q} with the rotation angle given by $\mathbf{Q}\mathbf{r}_j$. All spins in a plane perpendicular to \mathbf{Q} are co-aligned.

Unlike circularly polarized electromagnetic wave, which is transverse, in the absence of anisotropic interactions spin plane in the exchange spin spiral may have arbitrary orientation with respect to the propagation vector \mathbf{Q} (and the crystal lattice).

If spin ordering wave vector \mathbf{Q} is commensurate with some reciprocal lattice vector $\boldsymbol{\tau}$, i.e. there exist a whole number n such that $n\mathbf{Q} = \boldsymbol{\tau}$, then only n different values of spin rotation angle (mod 2π) are possible on the lattice and spin structure is commensurate spiral with finite repeat period. In this case there are only n different spin orientations in the crystal and one can divide the spin system into n sublattices with co-aligned spins and define a superlattice with larger unit cell which contains all differently aligned spins. A simple example is spin structure in a two-dimensional antiferromagnet on triangular lattice. It is a commensurate spin spiral with propagation vector $\mathbf{Q} = (1/3, 1/3)$ consisting of three sublattices directed at 120° to each other, cf. Figure 5(c). While sublattice description is straightforward, it entails significant complications for spin wave calculations and for understanding the structure and behavior of spin order parameter and excitations. Existence of n spin species requires n equations of motion, enlarged unit cell corresponds to a proportionally smaller Brillouin zone into which dispersion of all excitations existing in the system have to be folded. It also implies a number of extinction rules for nuclear Bragg peak intensities prohibiting unphysical peaks, which would be at fractional positions in the real lattice. Finally, sublattice description is not possible for incommensurate spirals.

While in some cases introducing spin sublattices is unavoidable, in many situations spin structure is a weakly distorted exchange spiral (14) and can be best described in terms of the nuclear lattice on which the spin Hamiltonian, e.g. (11), is defined. In this description all spins in the ordered structure are treated equally, without subdividing them into sublattices. The lattice unit cell is not increased to incorporate translational symmetry breaking by spin order. The corresponding folding of the nuclear Brillouin zone is also avoided. Instead, additional (magnetic) Bragg peaks corresponding to spin superlattice are indexed in the paramagnetic (nuclear) Brillouin zone. For a Bravais lattice there is a single branch of spin wave excitations, whose properties are determined by spin structure. A general procedure for finding the ground state structure of classical-spin Hamiltonian (11) on a simple Bravais lattice was developed in Refs. [28,29,30,31] and recently discussed in Refs. [32,33,34]. One has to minimize a function of N classical vector variables \mathbf{S}_j , subject to N constraints of equal length, $\mathbf{S}_j^2 = S^2$. Employing Lagrange multipliers and switching to Fourier representation, which takes advantage of lattice translational symmetry, the following system of equations for spin configuration, minimizing spin Hamiltonian (11) under the equal-spin constraint is obtained,

$$NJ_{\mathbf{q}}\mathbf{S}_{\mathbf{q}} + \mathbf{e}_z DS_{\mathbf{q}}^z - \sum_{\mathbf{q}'} \lambda_{\mathbf{q}'} \mathbf{S}_{\mathbf{q}-\mathbf{q}'} = \frac{\gamma}{2} \mathbf{H} \delta_{\mathbf{q},0}, \quad \sum_{\mathbf{q}'} \mathbf{S}_{\mathbf{q}'} \cdot \mathbf{S}_{\mathbf{q}-\mathbf{q}'} = S^2 \delta_{\mathbf{q},0}. \quad (15)$$

Here \mathbf{e}_z is the unit vector along z-axis, $\delta_{\mathbf{q},\mathbf{q}'}$ is a 3D Kronecker symbol, and $\mathbf{S}_{\mathbf{q}}$, $\lambda_{\mathbf{q}}$ and $J_{\mathbf{q}}$ are the lattice Fourier transforms of spin \mathbf{S}_j , Lagrange multiplier λ_j and exchange coupling $J_{jj'}$ lattice fields, e. g.,

$$J_{\mathbf{q}} = \sum_{\mathbf{r}_{jj'}} J_{jj'} e^{-i\mathbf{q}\cdot\mathbf{r}_{jj'}} = J_{-\mathbf{q}}, \quad J_{jj'} = \frac{1}{N} \sum_{\mathbf{q}} J_{\mathbf{q}} e^{i\mathbf{q}\cdot\mathbf{r}_{jj'}}. \quad (16)$$

Result (14) follows immediately from Eq. (15). In the absence of anisotropy and magnetic field, the ground state energy per spin is $E_{GS}/N = J_Q S^2$, so the ordering wave vector \mathbf{Q} corresponds to the minimum of the Fourier transform of exchange interaction, $J_Q = \min\{J_q\}$. When magnetic field \mathbf{H} is turned on in the absence of spin anisotropy ($D = 0$), spins simply tilt towards field, forming a cone. \mathbf{S}_Q and the plane of spin spiral component align perpendicular to the field, the net magnetization, $\gamma \mathbf{S}_0 = \chi \mathbf{H}$, is parallel to it. The same simple structure is realized when there is uniaxial anisotropy but magnetic field is parallel to its axis, although for easy-axis spin anisotropy ($D < 0$) it occurs only for fields above spin-flop transition field, $H > H_{sf} \sim S\sqrt{|D|J}$. The balance between exchange and Zeeman energy determines spin-canting (cone) angle α , $\sin \alpha = H/H_s$, which is valid up to the saturation field, $H_s = 2S(J_0 + J_Q + D)$. Above H_s , $\sin \alpha = 1$ and spins are aligned parallel to magnetic field.

In the general case, when both anisotropy and magnetic field are present, the situation is significantly more complicated. In addition to straightforward spin canting towards magnetic field as in simple cases mentioned above, a non-collinear classical spin spiral also becomes distorted. This distortion, known as “bunching”, is described by the appearance of Fourier harmonics at integer multiples, $n\mathbf{Q}$, of the spin structure ordering wave vector \mathbf{Q} , i. e. at $\mathbf{S}_{2\mathbf{Q}}$, $\mathbf{S}_{3\mathbf{Q}}$, etc., in addition to \mathbf{S}_Q . When such distortion is weak, e. g. for small D and H , it can be calculated using perturbative harmonic expansion,

$$\lambda_q = \sum_n \lambda_n \delta_{q,nQ}, \mathbf{S}_q = \sum_n \mathbf{S}_{nQ} \delta_{q,nQ}, \text{ where } \lambda_{n \neq 0} \sim O\left(\sqrt{\frac{D}{J}}, \frac{\mathcal{H}}{J}\right) \cdot \lambda_{|n|-1} \text{ and } |\mathbf{S}_{nQ}| \sim O(\lambda_{|n|-1})$$

[33]. Alternatively, it can be obtained by considering perturbative corrections to spiral

winding angle in the real-space spin structure, $\delta\theta_j = \sum_n \alpha_n \cos(n\mathbf{Q}\mathbf{r}_j) + \beta_n \sin(n\mathbf{Q}\mathbf{r}_j)$,

where the coefficients α_n and β_n are of the order $\sim O\left(\left(\frac{D}{J}\right)^n, \left(\frac{\mathcal{H}}{J}\right)^n\right)$ [32].

Squares of the absolute value of Fourier components of spin density, $|\mathbf{S}_{\mathbf{Q}}|^2$, $|\mathbf{S}_{2\mathbf{Q}}|^2$, etc., are proportional to the intensity of magnetic Bragg reflections associated with spin order at the corresponding wave vectors, \mathbf{Q} , $2\mathbf{Q}$, etc., which are measured in experiment, e.g. by magnetic neutron diffraction [35,36]. For spin structures on a simple Bravais lattice discussed above, where there is only one spin in the crystal unit cell, $\mathbf{S}_{\mathbf{Q}}$ is simply given by the magnitude of that spin S . Higher harmonics, which result from distortion of exchange spin structure, for small distortions can be calculated following the procedure described above, see e.g. Refs. [32,37]. For non-Bravais crystal lattices with several spins in the unit cell, $\mathbf{S}_{\mathbf{Q}}$ is the Fourier transform of the spin density of the whole unit cell. When there is more than one atom in the unit cell of the crystal, the above procedure of finding spin GS has to be modified by introducing several spin species. While this situation is actually more common in real materials, it leads to some computational complications, resulting in a system of linear equations for the order parameters of different spin species [35]. Nevertheless, the result in principle is not much different from that for Bravais lattice. In fact, spin structures can often be easily understood by simply considering bond energies contributing to the Hamiltonian (11).

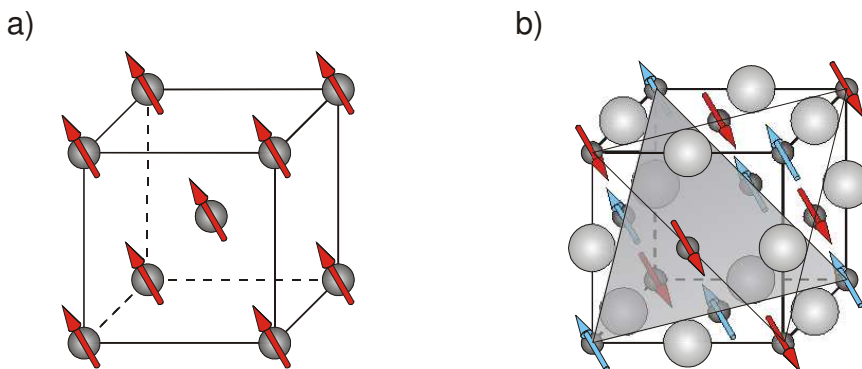


Figure 1. (a) Ferromagnetic spin alignment on the body-centered cubic (bcc) lattice found in simple metals (Fe, Ni, Co, ...). (b) Antiferromagnetic spin structure on the NaCl-type face-centered cubic (fcc) lattice found in metal monoxides such as FeO, NiO, CoO, MnO. Small darker spheres with arrows show metal ions and their spins, larger spheres are oxygen anions. Structure consists of ferromagnetic sheets perpendicular to (111) diagonal of the cubic unit cell (shown semi-transparent in the figure), staggered antiferromagnetically.

Some examples of spin structures found in different materials are shown in Figure 1 through Figure 4. The simplest, ferromagnetic structure, most commonly occurs in metals, such as 3*d* metals of the iron group, Figure 1(a). While electron states in metals form bands and applicability of the localized spin description is questionable, experiments do indicate existence of localized magnetic moments in metals of the iron group and their alloys, persisting well above the Curie temperature [38,39,40]. This can be visualized by adopting a simple approximate picture called *s-d* model, where electrons of the incomplete *d*-shell are localized, while valence *s*-electrons are involved in metallic cohesion and are collectivized and described by Bloch wave functions [17]. They provide long-range indirect exchange between the localized *d*-electrons. First-principle local spin density functional calculations [41] indicate that effective Heisenberg localized spin Hamiltonian can indeed be used for describing 3*d* metals, and give effective exchange parameters for iron and nickel which agree well with experimental values. However, experimentally determined magnetic moments in ferromagnetic 3*d* metals, $\mu_{\text{Fe}} \approx 2.2$, $\mu_{\text{Co}} \approx 1.7$, $\mu_{\text{Ni}} \approx 0.6$, are noticeably smaller than corresponding expected free-atom values

arising from spin of unpaired 3d electrons, $S_{\text{Fe}} = 2$, $S_{\text{Co}} = 3/2$, $S_{\text{Ni}} = 1$, which shows that simplistic *s-d* model is at best a very coarse approximation.

Transition metal monoxides with simple fcc crystal lattice adopt antiferromagnetic spin structure shown in Figure 1(b) [42]. It is driven by strong antiferromagnetic superexchange through 180° M-O-M (M = Fe, Ni, Co, Mn) bond. Propagation vector of such structure is $Q=(1/2,1/2,1/2)$, in reciprocal lattice units of the cubic lattice shown in the figure. Spin alignment, however, is different in different oxides, although except for CoO spins tend to be confined to [111] planes. Antiferromagnetic order at T_N is usually accompanied by a slight trigonal distortion arising from magnetostriction associated with anisotropic spin interactions, which makes the symmetry of the crystal consistent with that of the spin structure, [43,44,45,46]. NiO has the highest Neel temperature in the series, $T_N^{(\text{NiO})} \approx 524$ K, $T_N^{(\text{CoO})} \approx 298$ K, $T_N^{(\text{FeO})} \approx 198$ K, $T_N^{(\text{MnO})} \approx 118$ K.

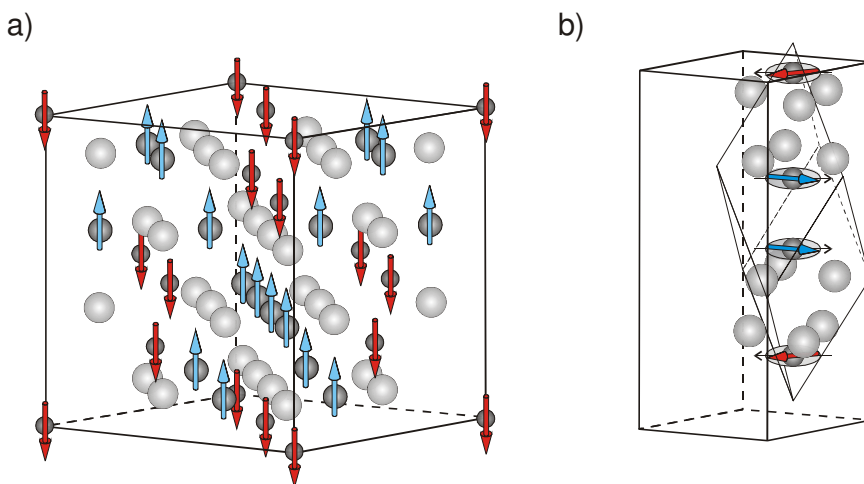


Figure 2. (a) Ferrimagnetic spin structure of magnetite, Fe_3O_4 . The unit cell contains 32 O^{2-} anions (larger light-shaded spheres) and 24 Fe cations (smaller dark spheres). 8 Fe^{3+} ions ($S = 2$) with co-aligned magnetic moments $\approx 4\mu_B$ occupy tetrahedrally co-ordinated sites (down arrows), while 16 octahedrally coordinated sites are occupied by an equal mixture of 8 Fe^{3+} and 8 Fe^{2+} ($S = 5/2$, $\mu \approx 5\mu_B$) ions aligned in the opposite direction (up arrows), resulting in net ferromagnetic moment $\approx 4\mu_B$ per unit cell, or $\approx 1/6\mu_B$ per iron. (b) Weak ferromagnetism in hematite, Fe_2O_3 . Nearly antiferromagnetic spins are shown slightly tilted in the basal plane, resulting in small ferromagnetic moment. Both hexagonal and the rhombohedral unit cell with four Fe^{3+} ions and oxygens bridging them are shown.

Apart from simple ferro- and antiferromagnetism shown in Figure 1, there are collinear spin structures where both parallel and antiparallel spin alignments co-exist, giving rise to an uncompensated net ferromagnetic, or more precisely ferrimagnetic moment. This can result from existence of atoms with different spins within the unit cell, such as Fe^{3+} and Fe^{2+} , which do not compensate each other when aligned antiferromagnetically, or from the combination of ferro- and antiferromagnetic spin alignment in the spin structure. In fact, both possibilities are realized in magnetite, Fe_3O_4 , which is a prototypical ferrimagnet known as lodestone since ancient times, Figure 2 (a). At room temperature the unit cell of magnetite contains three Fe_3O_4 formula units and 24 spins in total, which are unequally distributed between 8 tetrahedrally coordinated A sites (populated by Fe^{3+} , $S = 2$) and 16 octahedrally coordinated B sites (equally populated by 8 Fe^{3+} , $S = 2$ and 8 Fe^{2+} , $S = 5/2$). Antiferromagnetic superexchange J_{AB} between A and B sites passing through $\approx 125^\circ$ A-O-B bond leads to the antiparallel alignment of A and B spins within the unit cell. Unequal population of A and B sites results in the ferrimagnetic structure. Already large unit cell is not further increased by spin structure, and magnetic Bragg reflections appear on top of nuclear Bragg peaks [47]. Despite small value of the superexchange coupling, $J_{AB} \approx 2.35 \text{ meV} \approx 27 \text{ K}$ [48], magnetite orders at very high temperature, $T_C \approx 858 \text{ K}$. This can be expected for large $\text{Fe}^{2+}/\text{Fe}^{3+}$ spins and is consistent with spin-wave calculations [49].

In the rhombohedral structure of hematite, Fe_2O_3 , and escholaite, Cr_2O_3 , there are four Fe^{3+} ($S = 2$) ions in the unit cell and two types of bonds between them. In the antiferromagnetic structure below $T_N \approx 950 \text{ K}$ spins coupled by the superexchange passing through oxygen anions align antiferromagnetically, while those coupled directly

are co-aligned, Figure 2(b). Once again spin order does not break lattice translational symmetry and magnetic and nuclear Bragg peaks overlap [50]. Superexchange bond, which couples spins from different sublattices, passes through two oxygen triangles that are rotated by 60° with respect to each other and thus lacks inversion symmetry. This allows DM anisotropic contribution to superexchange, with \mathbf{D} vector parallel to the three-fold rotation axis (z -axis). As a result, spins from different sublattices can lower their energy by slightly canting towards each other and producing a weak ferromagnetic component in the basal plane, perpendicular to z -axis. The same weak ferromagnetism is also found in many other materials, e. g. MnCO_3 and CoCO_3 [51].

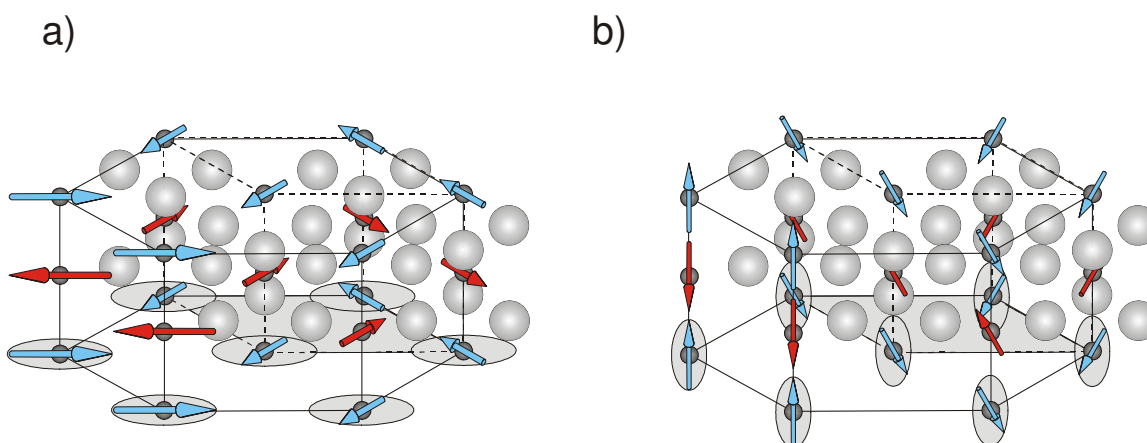


Figure 3. Triangular spin ordering in quasi-one-dimensional ABX_3 hexagonal perovskites; magnetic ordering wave vector is $\mathbf{Q} = (1/3, 1/3, 1)$. Dark spheres with arrows show $3d$ metal ions and their spin. Anions (X) bridging $3d$ ions in the chains at the corners one unit cell (dashed lines) and providing the exchange coupling are also shown (larger light spheres). (a) Easy-plane anisotropy does not distort 120° spin structure, simply forcing the plane of spin spiral to lie in the a - b basal plane. (b) Easy-axis anisotropy $\parallel c$ -axis not only forces spin plane to be perpendicular to the basal plane, but also distorts perfect 120° triangular ordering (e. g. in CsNiCl_3 the angle between the neighbor chains is $\approx 119^\circ$).

Perhaps, simplest non-collinear exchange spin structure is a 120° triangular spin ordering occurring in an antiferromagnet on the two-dimensional triangular lattice. It is also an example of the commensurate spin spiral with propagation vector $\mathbf{Q} = (1/3, 1/3)$. Such spin ordering is found in many magnetically quasi-one-dimensional perovskites of ABX_3 family ($A = \text{Cs, Rb, K, \dots}$, $B = \text{Ni, Mn, V, \dots}$, $X = \text{Cl, Br, I, \dots}$) with hexagonal crystal

structure. In these compounds antiferromagnetic spin chains consisting of $3d$ metal sites and running along the hexagonal C_6 axis are arranged on the triangular lattice in the basal plane and form a 120° triangular spin structure in this plane, Figure 3. Easy-plane anisotropy found e.g. in CsMnBr_3 and CsVBr_3 does not distort 120° exchange structure, simply forcing all spins into the basal plane [52,53]. In the case of easy-axis anisotropy (e. g. in CsNiCl_3 , RbNiCl_3 , CsMnI_3), spins lie in a plane containing z -axis. Triangular spin ordering of ideal spiral structure is distorted and spin opening angle is less than 120° [54]. In CsMnI_3 , where it is only 100° , magnetic Bragg peak corresponding to third order harmonics of spin spiral structure, $3\mathbf{Q} = (1,1,1)$, is readily observed [55].

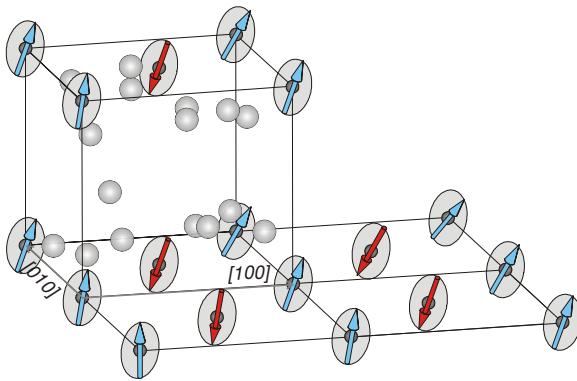


Figure 4. Spiral spin structure in quasi-2D antiferromagnet $\text{Ba}_2\text{CuGe}_2\text{O}_7$. Cu^{2+} ions (dark spheres) with $S=1/2$ spins (arrows) form ideal square lattice in the a - b plane. Larger, light-shaded spheres show oxygens in one unit cell. Non-centrosymmetric tetragonal crystal structure (space group $\text{P4}_2\text{1m}$) gives rise to Dzyaloshinskii-Moriya interaction which favors spiral spin arrangement with spins confined in $[1,-1,0]$ xz plane (x -axis is directed along the diagonal of the square) and magnetic propagation vector $(1+\zeta, \zeta, 0)$ with $\zeta \approx 0.0273$. This means that interacting nearest neighbor spins along the diagonal of the square unit cell rotate by $\alpha = 360^\circ \cdot \zeta \approx 9.8^\circ$ in xz plane with respect to their antiparallel alignment in the simple collinear antiferromagnetic structure with $\mathbf{Q} = (1,0,0)$.

An example of the incommensurate spiral spin structure resulting from Dzyaloshinsky-Moriya interaction is found in quasi-2D $S=1/2$ antiferromagnet $\text{Ba}_2\text{CuGe}_2\text{O}_7$ shown in Figure 4 [37,56]. Absence of the inversion symmetry of the antiferromagnetic bond between nearest neighbor spins on the centered square lattice in the basal plane allows uniform antisymmetric DM exchange with vector \mathbf{D} parallel to (001) z -axis. The spin

interaction energy is minimized when all spins are perpendicular to D , in which case exchange energy per bond is $2J \cos \varphi + D \sin \varphi = \sqrt{4J^2 + D^2} \cos(\varphi - \alpha)$, where J is the antiferromagnetic isotropic Heisenberg superexchange, $\alpha = -\arctan(D/J)$ and φ is the angle between the spins. The energy is a minimum for $\varphi = \pi + \alpha$ and the ground state spin structure is an incommensurate spin spiral with propagation vector $\mathbf{Q} = (1+\zeta, \zeta, 0)$, $\zeta = \alpha/(2\pi)$, shown in Figure 4. In this case not only spin alignment, but also spiral propagation vector are both determined by weak anisotropic interactions, and therefore both are equally strongly sensitive to magnetic field [58].

5. Spin Wave Excitations

Spin waves are usually understood in the framework of semi-classical description and can be visualized as small oscillations of classical spin vectors around their equilibrium positions in the ground state spin structure, as shown in Figure 5. Their wave-like spatial composition results from the translational symmetry of the system. Frequencies of spin wave oscillations can be calculated from spin Hamiltonian, e.g. Eq. (11), by writing torque equations of motion for classical spins [3]. Such approach relies entirely on classical mechanics and can be most generally pursued employing Poisson brackets formalism [59]. Spin waves are normal modes of the linearized equations of motion. They involve small spin deviations that are perpendicular to the equilibrium spin direction. Hence, spin waves are transversely polarized, with two mutually orthogonal linear polarizations of spin oscillations possible. A circular spin precession around its equilibrium position can have two possible directions, clockwise and counter-clockwise; one is shown in Figure 5(a) for a spin wave in ferromagnetic structure.

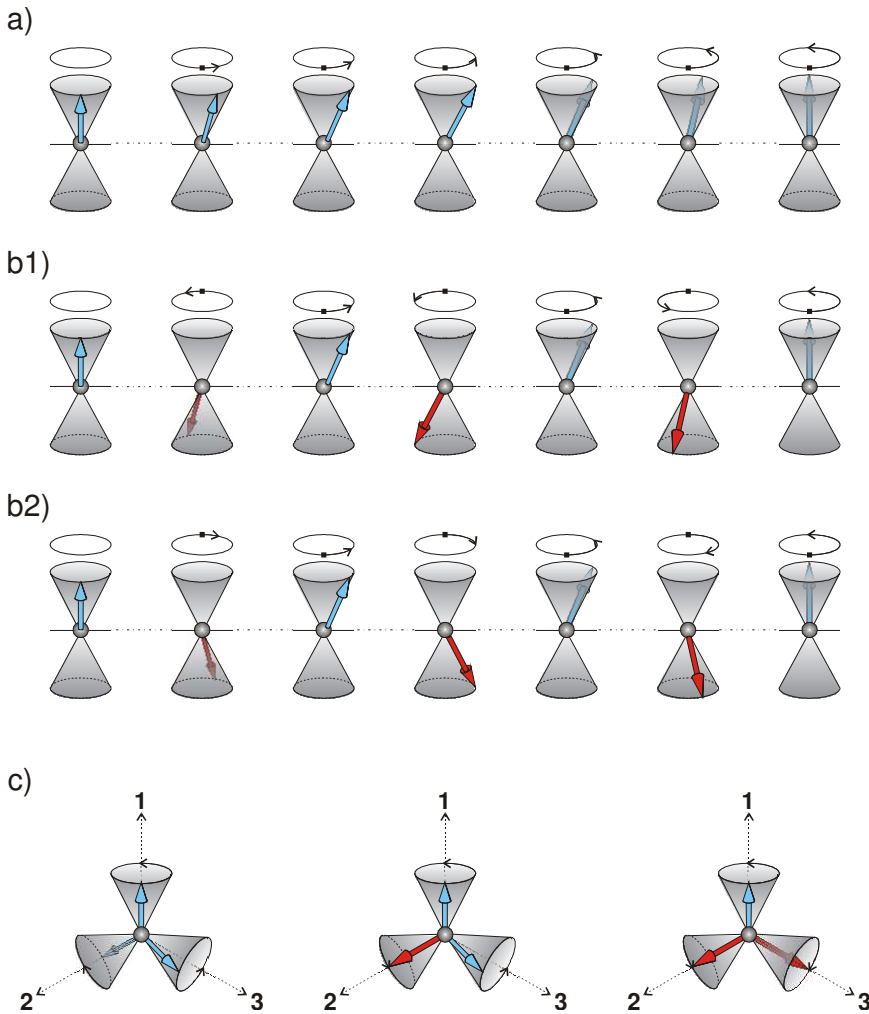


Figure 5. Spin waves in different spin structures. Each spin undergoes precession about its equilibrium direction sweeping out the surface of a cone over a period $2\pi/\omega(\mathbf{q})$, where $\omega(\mathbf{q})$ is frequency of spin wave and \mathbf{q} is the wave vector. (a) ferromagnet, (b1) in-phase and (b2) anti-phase mode in two-sublattice antiferromagnet, (c) in-phase and two anti-phase (left to right) modes in 3-sublattice antiferromagnet on triangular lattice. A half-period of spin-wave oscillation spanning 6 spins is shown in (a) and (b1,b2), corresponding to spin wave with wave vector equal to $1/12$ of reciprocal lattice unit in the direction of propagation. Anti-phase mode in (b2) corresponds to wave vector $7/12$ in the extended paramagnetic Brillouin zone description.

In an antiferromagnetic spin structure, precession of two sublattices can have the same, Figure 5(b1), or the opposite sense, Figure 5(b2). In the sublattice description, where magnetic superlattice contains two spin species, these correspond to two distinct, in-phase and anti-phase, spin wave modes. In the extended, paramagnetic Brillouin zone (BZ) description, where there is only one spin wave branch for spins on a Bravais lattice, these two modes correspond to spin waves having different wave vectors, \mathbf{q} and $\mathbf{q} \pm \mathbf{Q}$,

where \mathbf{Q} is the antiferromagnetic ordering wave vector. For a 3-sublattice antiferromagnetic spin structure on triangular lattice there are two possible choices of sublattice(s) rotating in the “wrong” sense. Hence, there are three spin wave modes, Figure 5(c). In general, the total number of spin wave modes in the sublattice description equals the number of sublattices. For a Bravais nuclear lattice, multiple modes arise from folding of the dispersion surface of a single mode defined in the large nuclear Brillouin zone into a small BZ of magnetic superlattice. Hence, their number is given by the volume ratio of these BZ.

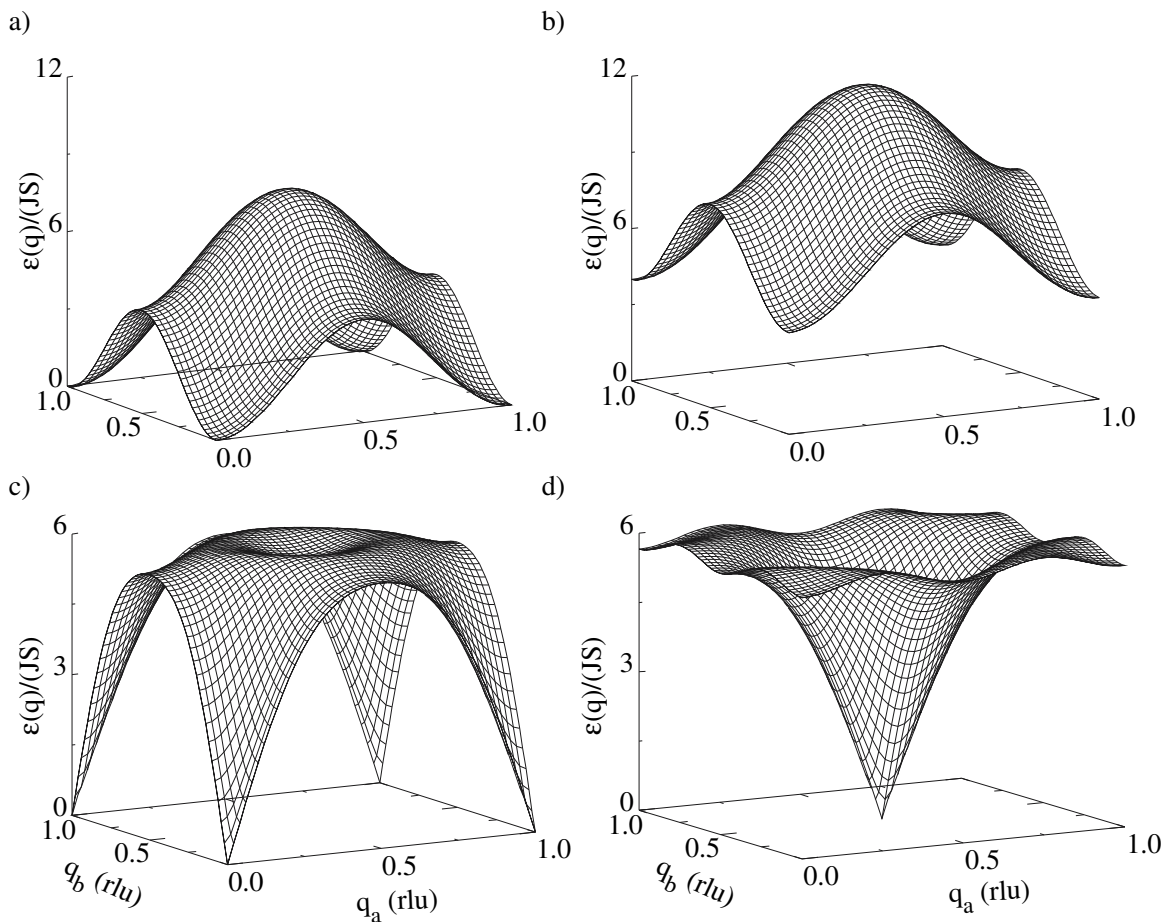


Figure 6. Cuts of the spin-wave dispersion surface in a ferromagnet, $J_a = J_b = J_c = J < 0$, (a),(b) and an antiferromagnet, $J_a = J_b = J_c = J > 0$, (c),(d) on a three-dimensional (3D) Bravais cubic lattice by an (h,k,l_0) reciprocal lattice plane with $l_0=0$ (left column, (a) and (c)) and $l_0=0.5$ (right column, (b) and (d)). Wave vector is measured in reciprocal lattice units (rlu), $q_a=h$, $q_b=l$. (a) Spin structure of a ferromagnet has propagation vector $\mathbf{Q}=(0,0,0)$ and magnetic Bragg peak positions coincide with

nuclear structure Bragg peaks at the corners of the Brillouin zone. A cosine-like dispersion is quadratic in \mathbf{q} around these points. (b) Dispersion for $\mathbf{Q}=(\mathbf{h},\mathbf{k},0.5)$ does not pass through $\mathbf{Q}=\mathbf{0}$ magnetic ordering vector and has a gap. (c) Dispersion in $\mathbf{Q}=(\mathbf{h},\mathbf{k},0)$ zone does not pass through $\mathbf{Q}=(1/2,1/2,1/2)$ magnetic ordering vector of an antiferromagnet but still softens for the uniform mode at $\mathbf{Q}=\mathbf{0}$ and has no gap. (d) Dispersion in $\mathbf{Q}=(\mathbf{h},\mathbf{k},1/2)$ zone cuts through the Goldstone mode with sin-like dispersion linear in the vicinity of magnetic ordering vector $\mathbf{Q}=(1/2,1/2,1/2)$.

In quantum mechanical description of spins, elementary quanta of spin excitation in spin systems, which in virtue of Eq. (1) are also elementary magnetic excitations, are known as magnons. In quantum mechanics, states of an isolated spin system on a lattice are specified by the total spin of the system, S_{tot} , its z -component, S_{tot}^z , and wave vector \mathbf{q} , which determines the eigenvalue of the lattice translation operator, $T_{\mathbf{r}}$,

$$T_{\mathbf{r}} \left| \mathbf{q}, S_{tot}, S_{tot}^z \right\rangle = e^{i\mathbf{q}\cdot\mathbf{r}} \left| \mathbf{q}, S_{tot}, S_{tot}^z \right\rangle. \quad (17)$$

A ground state for an isotropic saturated ferromagnet is $\left| 0, NS, S_{tot}^z \right\rangle$, $-NS < S_{tot}^z < NS$.

For an antiferromagnet it is $\left| 0,0,0 \right\rangle$ (this implies sublattice description; ordered GS is doubly degenerate). In many cases this set of quantum numbers is sufficient for describing low-energy states of the system, which can differ from the ground state by having a non-zero \mathbf{q} and by the value of the total spin, i. e. $\Delta S_{tot}^z = 0, \pm 1$. Therefore, quantum magnons describing these states are specified by wave vector, \mathbf{q} , and spin, $S = 1, S^z = 0, \pm 1$, quantum numbers. Clearly, there are three magnon polarizations in quantum theory, as opposed to only two for transverse spin waves in classical description. However, in systems where semi-classical description is valid, e. g. for $S \gg 1$, and spin order is well-developed, only two magnons corresponding to semi-classical spin waves are relevant.

Except for few specific important cases, full quantum-mechanical treatment of spin Hamiltonian presents insurmountable difficulties [3]. The most successful approximate

approach to treating quantum spins is the spin wave theory, which starts from a semi-classical approximation and is based on a perturbative expansion in $1/S$. Semi-classical magnons obtained in the leading, first-order perturbation of spin wave theory are just classical spin waves.

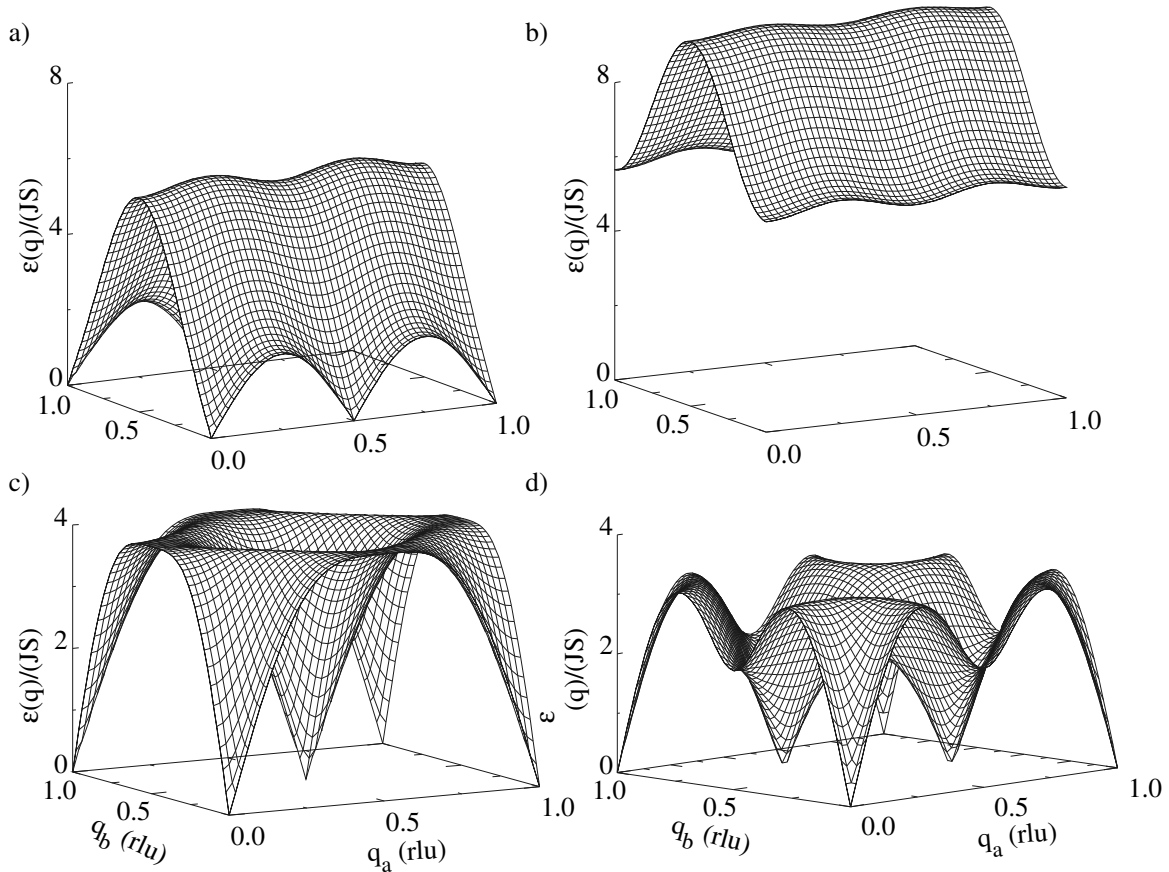


Figure 7. (a,b) Spin-wave dispersion in an antiferromagnet on the 3D cubic Bravais lattice with $J_a = -J_b = -J_c = J > 0$, i.e. ferromagnetic layers in b-c plane stacked antiferromagnetically along a. (a) cut by an $(h,k,0)$ reciprocal lattice plane showing a Goldstone mode with sine-like dispersion along a arising from magnetic ordering vector $Q = (0.5,0,0)$. (b) cut by an $(h,k,0.5)$ plane containing neither $Q=0$ nor $Q = (0.5,0,0)$ and therefore no soft modes. (c) Spin-wave dispersion in a 2D antiferromagnet on a square lattice. There are two soft modes, at $Q = 0$ and at the magnetic ordering vector $Q = (1/2,1/2)$. (d) spin waves in a triangular lattice antiferromagnet. In addition to soft mode at $Q = 0$, there are two Goldstone modes at two equivalent spin ordering wave vectors, $Q = (1/3,1/3)$ and $Q = (2/3,2/3)$.

In spin-wave theory spins are quantized by expanding deviations from their equilibrium directions in the classical spin structure in series of Bose creation-annihilation operators, using e. g. Holstein-Primakoff transformations [60]. Energies of spin excitations and

quantum corrections to spin structure can then be calculated using perturbation theory for a system of interacting bosons. A rather complete non-linear spin-wave theory accounting for second and higher order perturbation corrections has been developed for the isotropic Heisenberg Hamiltonian, some examples are found in Refs. [61-64].

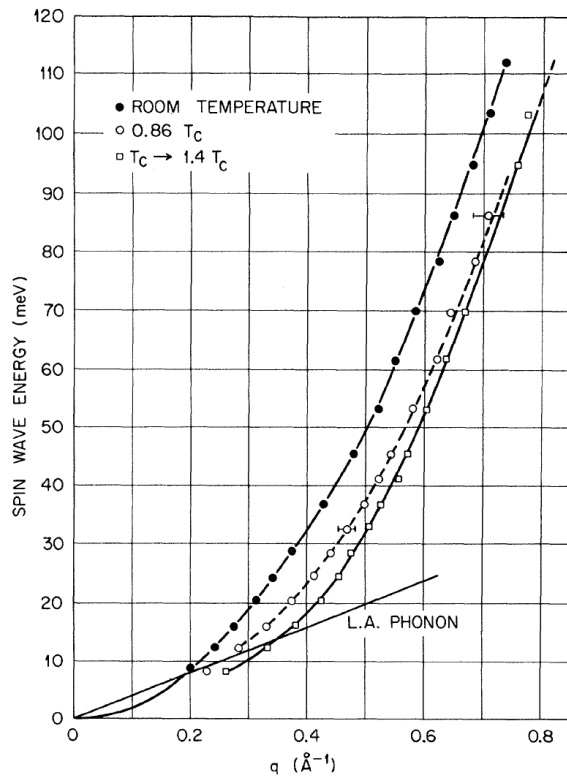


Figure 8. Dispersion of spin waves in Fe with 12 at. % of Si at several temperatures, measured by J. W. Lynn using unpolarized inelastic neutron scattering [40]. With increasing temperature spin wave energy somewhat softens, but, outside a small hydrodynamic region, spin-waves neither disappear, nor their dispersion renormalizes to zero as $T \rightarrow T_C$, indicating existence of localized spins.

Spin wave calculations proceed by transforming every spin operator to its own co-ordinate system with z -axis pointing along the spin direction in the classical ground state spin structure. For a co-planar exchange spiral (14), such co-ordinate transformation is achieved by a rotation through an angle $\mathbf{Q}\mathbf{r}_j$. Then, in order to obtain the first $1/S$ correction to classical approximation, in the standard perturbation scheme spin operators are expressed through boson operators, a^+, a , by employing the truncated Holstein-

Primakoff transformation, $S_j^z = S - a^+ a$, $S_j^+ \approx a\sqrt{2S}$, $S_j^- \approx a^+\sqrt{2S}$. The first-order corrections in such a linear, or harmonic spin wave theory appear in the form of quadratic boson Hamiltonian describing system of quantum oscillators, which correspond to quantized classical spin waves. Applying this procedure to Hamiltonian (11) for spin spiral without harmonic distortions, the following boson equivalent is obtained, [34],

$$H = \sum_{\mathbf{q}} \left\{ (A_{\mathbf{q}} + C_{\mathbf{q}}) a_{\mathbf{q}}^+ a_{\mathbf{q}} + \frac{1}{2} B_{\mathbf{q}} (a_{\mathbf{q}} a_{-\mathbf{q}} + a_{\mathbf{q}}^+ a_{-\mathbf{q}}^+) \right\}, \quad (18)$$

where

$$A_{\mathbf{q}} = -2SJ_{\mathbf{Q}} + S \cos^2 \alpha (J_{\mathbf{q}} + D) + S(1 + \sin^2 \alpha) \frac{J_{\mathbf{q}+\mathbf{Q}} + J_{\mathbf{q}-\mathbf{Q}}}{2},$$

$$B_{\mathbf{q}} = -S \cos^2 \alpha \left(J_{\mathbf{q}} + D - \frac{J_{\mathbf{q}+\mathbf{Q}} + J_{\mathbf{q}-\mathbf{Q}}}{2} \right), \quad C_{\mathbf{q}} = S \sin \alpha (J_{\mathbf{q}+\mathbf{Q}} - J_{\mathbf{q}-\mathbf{Q}}).$$

$A_{\mathbf{q}}$ and $B_{\mathbf{q}}$ are even, while $C_{\mathbf{q}}$ is an odd function of \mathbf{q} . Eq. (18) is diagonalized by the standard Bogolyubov transformation (which leaves odd- \mathbf{q} terms unchanged), resulting in

$$\text{the Hamiltonian of uncoupled harmonic oscillators, } H = \sum_{\mathbf{q}} \left\{ \varepsilon(\mathbf{q}) \left(a_{\mathbf{q}}^+ a_{\mathbf{q}} + \frac{1}{2} \right) - \frac{1}{2} A_{\mathbf{q}} \right\}.$$

The constant term $\sum_{\mathbf{q}} \frac{1}{2} (\varepsilon(\mathbf{q}) - A_{\mathbf{q}})$ gives $1/S$ quantum correction to the classical ground state energy. The energy of semi-classical magnons is $\varepsilon(\mathbf{q}) = \sqrt{A_{\mathbf{q}}^2 - B_{\mathbf{q}}^2} + C_{\mathbf{q}}$, or,

$$\varepsilon(\mathbf{q}) = 2S \sqrt{\left(\frac{J_{\mathbf{q}+\mathbf{Q}} + J_{\mathbf{q}-\mathbf{Q}}}{2} - J_{\mathbf{Q}} \right) \left(\frac{J_{\mathbf{q}+\mathbf{Q}} + J_{\mathbf{q}-\mathbf{Q}}}{2} \sin^2 \alpha + (D + J_{\mathbf{q}}) \cos^2 \alpha - J_{\mathbf{Q}} \right)}. \quad (19)$$

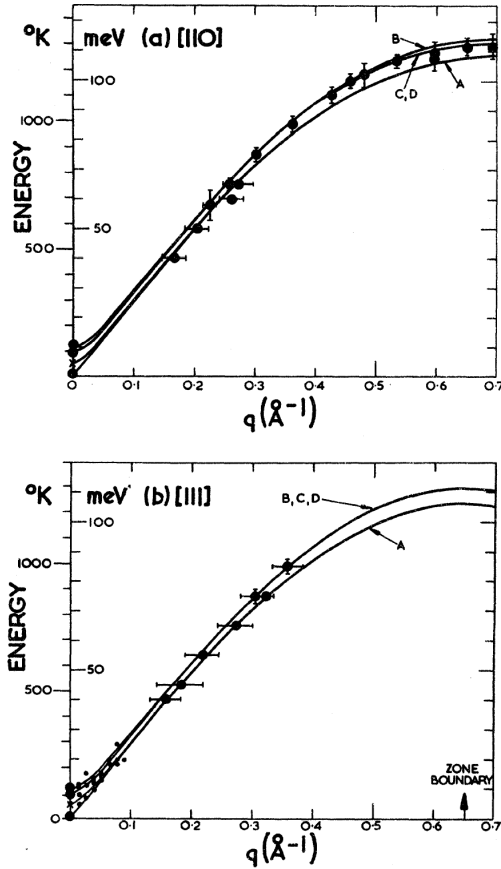


Figure 9. Dispersion of spin waves in antiferromagnetic NiO at $T = 78$ K, (a) along (110) and (b) along (111) reciprocal lattice directions, measured by Hutchings and Samuelsen in Ref. [65]. Wave vector is indexed in small Brillouin zone of magnetic superlattice with 4-times enlarged unit cell, such that magnetic ordering wave vector is $\mathbf{Q} = (1,1,1)$. Different curves marked A, B, C, and D show spin wave calculation for different magnetic domains corresponding to four possible symmetrically equivalent directions of \mathbf{Q} in the cubic lattice.

According to Goldstone's theorem, breaking of a continuous symmetry of the

Hamiltonian in the ground state must entail a zero energy mode(s) in the excitation

spectrum. Such modes appear in the spin wave dispersion of Eq. (19) at $\mathbf{q} = 0$ and at $\mathbf{q} =$

\mathbf{Q} , the latter only has zero energy in the absence of anisotropy and magnetic field.

Dispersion of spin wave excitations in different spin structures on simple Bravais lattices

calculated using Eq. (19) for $H = D = 0$ and for nearest neighbor spin interaction are

shown in Figure 6 and Figure 7. Fourier transformed exchange is obtained by summing

over the neighbor bonds, $J_{\mathbf{q}} = \sum_{\mathbf{d}} 2J_{\mathbf{d}} \cos(\mathbf{q} \cdot \mathbf{d})$, which for a simple cubic lattice is just

$J_a \cos 2\pi q_a + J_b \cos 2\pi q_b + J_c \cos 2\pi q_c$. For a ferromagnet, where $\mathbf{Q} = 0$, this expression simply has to be shifted upwards by $J_0 = J_a + J_b + J_c$ to obtain the spin wave spectrum shown in Figure 6(a),(b). There is a Goldstone mode with quadratic dispersion at $\mathbf{q} = 0$.

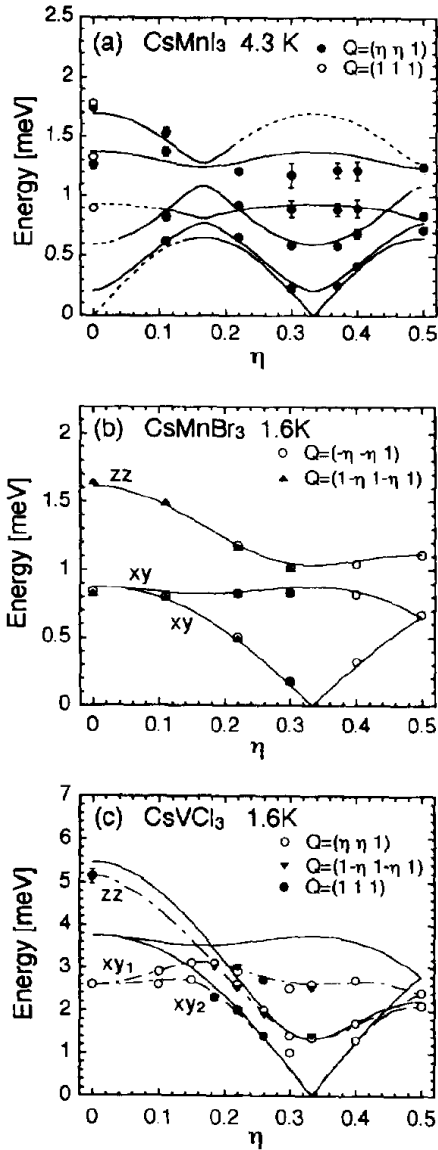


Figure 10. Spin wave dispersion in the a - b basal plane in several hexagonal quasi-1D antiferromagnets with 120° triangular spin structure measured by Inami et. al. in Ref. [53].

Inelastic neutron scattering provides a direct way of studying spin waves in most magnetic materials. Magnetic neutron scattering cross-section is directly proportional to the dynamic spin susceptibility and exhibits sharp, delta function-like peaks at spin wave

energies [35,36]. Quadratic spin wave dispersion measured by J. W. Lynn in ferromagnetic iron is shown in Figure 8. Spin waves persisting at elevated temperatures, up to and above the Curie temperature, indicate existence of localized spins. Quadratic in q dispersion is, in fact, a very general consequence of the existence of net ferromagnetic moment in the spin system, and therefore it is also observed in ferrimagnets [37].

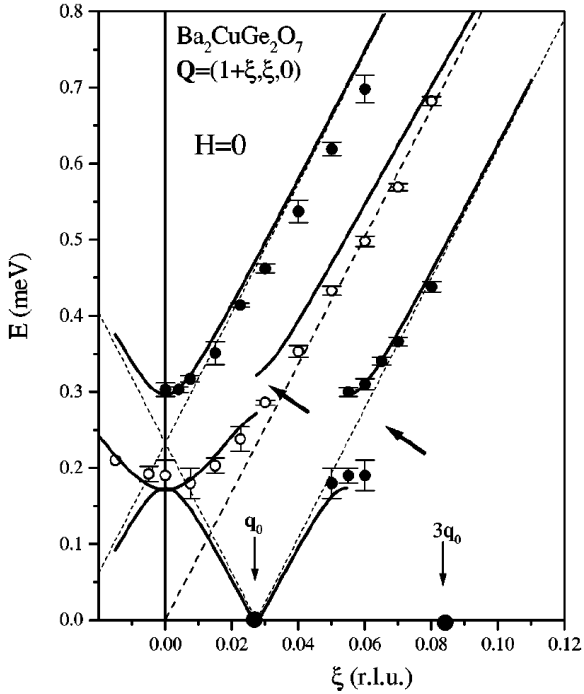


Figure 11. Dispersion of spin waves in Dzyaloshinski-Moriya spiral spin structure found in $\text{Ba}_2\text{CuGe}_2\text{O}_7$ in zero magnetic field, measured at $T = 0.35$ K by Zheludev et. al. in Ref. [37]. The filled circles on the abscissa axis show positions of the observed magnetic Bragg peaks at Q and $3Q$. The solid curves are parameter-free theoretical curves resulting from spin-wave theory calculation.

In antiferromagnets and helimagnets (spin spirals) spin wave dispersion of Goldstone modes is linear. For an antiferromagnet on a Bravais cubic lattice, cuts of the dispersion surface by planes perpendicular to $[001]$ direction intercept only one Goldstone mode at a time, Figure 6(c),(d). The situation is different in ferro-antiferromagnet, which is made of ferromagnetic sheets in b - c plane coupled antiferromagnetically along a , Figure 7(a),(b). The antiferromagnetic, sine-like dispersion is pronounced along a -axis, while

ferromagnetic dispersion in b - c plane is only modified to produce linear spectrum of a Goldstone mode in the vicinity of the ordering wave vector, $\mathbf{Q} = (1/2, 0, 0)$.

A sine-like dispersion of spin waves in the prototypical antiferromagnet NiO measured by Hutchings and Samuelsen in Ref. [65] is shown in Figure 9. Data in the figure is indexed in the reduced Brillouin zone of magnetic superlattice, which contains a number of modes whose dispersions coincide.

Spin wave dispersion in a 2D antiferromagnet on square lattice is shown in Figure 7, (c). Such system attracted considerable attention after antiferromagnetism was discovered in the un-doped parent materials of high-temperature superconducting cuprates, La_2CuO_4 [66] and $\text{Y}_2\text{BaCu}_3\text{O}_{6+x}$, [67] where weakly coupled layers of Cu^{2+} ions form square lattice in the basal a - b plane of the tetragonal crystal structure. Exchange coupling through 180° Cu-O-Cu bond is extremely strong, reaching ~ 0.23 meV in chain cuprates [68]. Hence, spin excitations are the most energetic eigenmodes and are crucial to understanding properties of cuprate materials. Recent advent of high-power pulsed spallation neutron sources utilizing time-of-flight spectroscopy enabled direct experimental observation of such excitations. Spectacular data on spin excitations in La_2CuO_4 reported in Ref. [69] was successfully described by spin waves, using effective localized spin Hamiltonian with superexchange and additional cyclic exchange induced by electron itinerancy. Similar measurements of high-energy excitations in superconducting $\text{Y}_2\text{BaCu}_3\text{O}_{6+x}$ reported in Ref. [70] can also reasonably well interpreted within the spin wave framework. These finding are quite surprising in view of the quantum nature of Cu^{2+} spins ($S=1/2$) and the low-dimensional (2D) character of these systems, undermining the mean field approach.

Spin wave dispersion in a 2D antiferromagnet on triangular lattice is shown in Figure 7 (d). In addition to $\mathbf{q} = 0$ and $\mathbf{q} = \mathbf{Q} = (1/3, 1/3)$, there is also a Goldstone mode at $\boldsymbol{\tau} - \mathbf{Q} = (2/3, 2/3) = 2\mathbf{Q}$, $\boldsymbol{\tau} = (1, 1)$ is a reciprocal lattice vector. This coincidence (up to $\boldsymbol{\tau}$) between \mathbf{Q} and $2\mathbf{Q}$ makes purely 2D triangular lattice a singular case. For one, harmonic expansion reduces to a single relation and cannot be used to describe bunching of triangular spin structure in magnetic field. Second, spin-wave calculations up to a second order in $1/S$ reveal dramatic modification of spin wave spectrum [71]. These complications are absent in quasi-1D hexagonal ABX_3 antiferromagnets with nearly triangular 120° spin structures, [52,53,54] where leading interaction is the in-chain exchange perpendicular to triangular lattice and the ordering wave vector is essentially 3D, $\mathbf{Q} = (1/3, 1/3, 1) \neq 2\mathbf{Q} = (2/3, 2/3, 0)$. Numerous neutron scattering studies of spin excitations in these materials indicate that for spin $S > 1$ they are reasonably well described by linear spin wave theory. Some experimental examples presented in Ref. [53] are reproduced in Figure 10. Resemblance of the data with dispersion of Eq. (19) shown in Figure 7(d) is clearly identifiable.

Perhaps, the most spectacular success of applying spin wave description to excitations in a spin system is presented in Figure 11. It reproduces spin wave spectrum in Dzyaloshinsky-Moriya spiral magnet $Ba_2CuGe_2O_7$, whose structure is shown in Figure 4 and was discussed above, measured by A. Zheludev, et. al., in Ref. [37]. Antisymmetric DM exchange in this material is accompanied by a two-ion anisotropy, and the resulting spin ground state is an incommensurate bunched spiral, with clearly observable magnetic Bragg peaks corresponding to third harmonics, $3\mathbf{Q}$, of the ordering wave vector \mathbf{Q} .

Distortion of spin spiral results in appearance of discontinuities in the spin wave dispersion at wave vectors $n\mathbf{Q}$, which are clearly observed in experiment.

6. Summary

Although magnetism is rooted in the quantum-mechanical nature of electron's spin, spin structures and excitations in great variety of magnetic materials can be successfully understood and often accurately described on the basis of semi-classical treatment of a localized spin Hamiltonian. Dispersion of spin excitations predicted by spin-wave theory agrees surprisingly well with experiment even for ordered spin system with $S=1/2$, where $1/S$ expansion is clearly not a good approximation. The fundamental reason for this is perhaps simply the fact that while the mapping of spin operators to bosons employed in different flavors of spin wave theory might not be entirely correct, the fundamental nature of spin excitations as coupled oscillators on a lattice is captured correctly. The resulting equations of motion and corresponding boson Hamiltonian are therefore also correct.

However, they may involve effective interaction parameters which can differ significantly from those in the original spin Hamiltonian and which are prescribed by the spin-wave approximation. Therefore, while reasons for the success of semi-classical spin-wave description might be superficial, similar to the Weiss theory of ferromagnetism, it provides a very useful parameterization for describing spin structures and excitations in magnetic materials, e.g. in the form of Eq. (18).

References.

1. A. Einstein, and W. J. De Haas, *Experimenteller Nachweis der Ampereschen Molekularströme (Experimental Proof of Ampere's Molecular Currents)*, Verhandlungen der Deutschen physikalischen Gesellschaft **17**, 152-170, 203 (1915).
2. S. J. Barnett, *Gyromagnetic and Electron-Inertia effects*, Rev. Mod. Phys. **7**, 129 (1935).
3. D. C. Mattis, *The Theory of Magnetism*, Harper & Row, New York (1965).
4. A. H. Compton, J. Franklin Inst. **192**, 144 (1921).
5. G. Uhlenbeck and S. Goudsmith, Naturwiss. **13**, 953 (1925).
6. Abragam, A., Bleaney, B., *Electron Paramagnetic Resonance of Transition Ions*. Dover Publications, New York (1986).
7. A. F. Andreev, Sov. Phys. JETP **47(2)**, 411 (1978).
8. P. A. M. Dirac, Proc. Roy. Soc. **112A**, 661 (1926).
9. W. Heisenberg, Z. Physik **38**, 441 (1926); *ibid.* 49, 619 (1928).
10. Bethe, Hans A., Jackiw, Roman, *Intermediate Quantum Mechanics*. Addison-Wesley, Massachusetts, USA (1997).
11. Yosida, K., *Theory of Magnetism*. Springer-Verlag, Berlin (1998).
12. J. H. Van Vleck, Rev. Mod. Phys. **17**, 27 (1945).

13. H. A. Kramers, *Physica* **1**, 191 (1934).
14. P. W. Anderson, *Phys. Rev.* **115**, 2 (1959).
15. J. Kanamori, *Phys. Chem. Solids* **10**, 87 (1959).
16. R. M. White, *Quantum Theory of Magnetism*, Springer-Verlag, Berlin (1983).
17. C. Zener, *Phys. Rev.* **81**, 440 (1959); *ibid.* **82**, 403 (1951).
18. T. Kasuya, *Progr. Theor. Phys.* **16**, 45 (1956).
19. K. Yosida, *Phys. Rev.* **106**, 893 (1957).
20. A. F. Andreev, V. I. Marchenko, *Sov. Phys. Usp.* **23**, 21 (1980).
21. J. Jensen, A. R. Mackintosh, *Rare Earth Magnetism*. Clarendon Press, Oxford (1991).
22. I. Dzyaloshinsky, *J. Phys. Chem. Solids* **4**, 241 (1958).
23. T. Moriya, *Phys. Rev.* **120**, 91 (1960).
24. N. D. Mermin and H. Wagner *Phys. Rev. Lett.* **17**, 1133-1136 (1966); *ibid.* **17**, 1307 (1966).
25. F. D. M. Haldane, *Phys. Rev. Lett.* **50**, 1153-1156 (1983).
26. P. Chandra, B. Doucot, *Phys. Rev. B* **38**, 9335 (1988).
27. P. W. Anderson, *Phys. Rev.* **86**, 694 (1952).

28. T. Nagamiya, in *Solid State Physics*, ed. F.~Seitz, D.~Turnbull and H.~Ehrenreich, **20**, 305, Academic Press, New York, 1967); T. Nagamiya, T. Nagata, and Y.~Kitano, *Progr. Teor. Phys.* **27**, 1253 (1962).
29. A. Yoshimori, *J. Phys. Soc. Jpn.* **14**, 807 (1959).
30. J. Villain, *J. Phys. Chem.* **11**, 303 (1959).
31. T. A. Kaplan, *Phys. Rev.* **116**, 888-889 (1959); T. A. Kaplan, *ibid.* **124**, 329 (1961).
32. I. A. Zaliznyak and M. E. Zhitomirsky, cond-mat/0306370; *JETP* **81(3)**, 579 (1995).
33. I. A. Zaliznyak, *Phys. Rev. B* **68**, 134451 (2003).
34. M. E. Zhitomirsky and I. A. Zaliznyak, *Phys. Rev. B* **53**, 3428 (1996).
35. Izyumov, Yu. A., and Ozerov, R. P., *Magnetic Neutron Diffraction*. New York: Plenum Press (1970).
36. I. A. Zaliznyak and S.-H. Lee, in *Modern Techniques for Characterizing Magnetic Materials*, Ed. Yimei Zhu, Springer, Heidelberg, New York (2005).
37. A. Zheludev, S. Maslov, G. Shirane, I. Tsukada, T. Masuda, K. Uchinokura, I. Zaliznyak, R. Erwin, L.-P. Regnault, *Phys. Rev. B* **59**, 11432 (1999); *Phys. Rev. Lett.* **81**, 5410 (1998).
38. P. J. Schurer, G. A. Sawatzky, F. van der Woude, *Phys. Rev. Lett.* **27**, 586-589 (1971).

39. P. J. Brown, H. Capellmann, J. Deportes, D. Givord, K. R. A. Ziebeck, J. Magn. Mater. **30**, 243 (1982).
40. J. W. Lynn, Phys. Rev. Lett. **52**, 775 (1984); Phys. Rev. B **11**, 2624 (1975).
41. A. Liechtenstein, M. I. Katsnelson, V. P. Antropov, V. A. Gubanov, J. Magn. Mater. **67**, 65 (1986).
42. C. G. Shull, W. A. Strauser, E. O. Wollan, Phys. Rev. **83**, 333 - 345 (1951).
43. G. E. Kugel, B. Hennion, C. Carabatos, Phys. Rev. B **18**, 1317 (1978).
44. K. Tomiyasu, T. Inami, N. Ikeda, Phys. Rev. B **70**, 184411 (2004).
45. A. Barbier, C. Mocuta, W. Neubeck, M. Mulazzi, F. Yakhou, K. Chesnel, A. Sollier, C. Vettier, F. de Bergevin, Phys. Rev. Lett. **93**, 257208 (2004).
46. A. L. Goodwin, M. G. Tucker, M. T. Dove, D. A. Keen, Phys. Rev. Lett. **96**, 047409 (2006).
47. C. G. Shull, E. O. Wollan, W. C. Koehler, Phys. Rev. **84**, 912-921 (1951).
48. H. A. Alperin, O. Steinsvoll, R. Nathans, G. Shirane, Phys. Rev. **154**, 508 (1951).
49. R. E. Mills, R. P. Kenan, F. J. Milford Phys. Rev. **145**, 704-717 (1966).
50. R. Nathans, S. J. Pickart, H. A. Alperin, P. J. Brown, Phys. Rev. **136**, A1641 (1964).
51. A. S. Borovik-Romanov, JETP **9**, 539 (1959).

52. M. Eibshutz, R. C. Sherwood, F. S. L. Hsu, D. E. Cox, AIP Conf. Proc. 17, 864 (1972).
53. T. Inami, K. Kakurai, H. Tanaka, M. Enderle, M. Steiner, Physica B **213&214**, 167 (1995).
54. W. B. Yelon and D. E. Cox, Phys. Rev. B **6**, 204 (1972); *ibid.* **7**, 2024 (1973).
55. A. Harrison, M. F. Collins, J. Abu-Dayyeh, C. V. Stager, Physical Review B **43** 679 (1991).
56. A. Zheludev, G. Shirane, Y. Sasago, N. Kiode, K. Uchinokura, Phys. Rev. B **54**, 15163 (1996).
57. A. Zheludev, S. Maslov, G. Shirane, Y. Sasago, N. Koide, K. Uchinokura, Phys. Rev. Lett. **78**, 4857 (1997).
58. A. Zheludev, S. Maslov, G. Shirane, Y. Sasago, N. Koide, K. Uchinokura, Phys. Rev. Lett **78**, 4857 (1997).
59. I. E. Dzyaloshinsky and G. E. Volovick, Ann. Phys. **125**, 67 (1979).
60. T. Holstein and H. Primakoff, Phys. Rev. **58**, 1098 (1940).
61. F. J. Dyson, Phys. Rev. **102**, 1217-1230 (1956).
62. A. V. Chubukov, J Phys. C **17**, L991 (1984); E. Rastelli, L. Reatto, A. Tassi, *ibid.* **18**, 353 (1985).
63. T. Ohyama and H. Shiba, J. Phys. Soc. Jpn. **62**, 3277 (1993); **63**, 3454 (1994).

64. M. Y. Veillette, A. J. James, and F. H. Essler, *Physical Review B* **72** 134429 (2005).
65. M. T. Hutchings and E. J. Samuelsen, *Phys. Rev. B* **6**, 3447 (1972).
66. D. Vaknin, S. K. Sinha, D. E. Moncton, D. C. Johnston, J. M. Newsam, C. R. Safinya, H. E. King, Jr., *Phys. Rev. Lett.* **58**, 2802 (1987).
67. J. M. Tranquada, D. E. Cox, W. Kunnmann, H. Moudden, G. Shirane, M. Suenaga, P. Zolliker, D. Vaknin, S. K. Sinha, M. S. Alvarez, A. J. Jacobson, D. C. Johnston, *Phys. Rev. Lett.* **60**, 156 (1988).
68. I. A. Zaliznyak, H. Woo, T. G. Perring, C. L. Broholm, C. D. Frost, and H. Takagi *Physical Review Letters* **93**, 087202 (2004).
69. R. Coldea, S. M. Hayden, G. Aeppli, T. G. Perring, C. D. Frost, T. E. Mason, S.-W. Cheong, and Z. Fisk, *Phys. Rev. Lett.* **86**, 5377 (2001).
70. C. Stock, W. J. L. Buyers, R. A. Cowley, P. S. Clegg, R. Coldea, C. D. Frost, R. Liang, D. Peets, D. Bonn, W. N. Hardy, and R. J. Birgeneau, *Phys. Rev. B* **71**, 024522 (2005).
71. O. A. Starykh, A. V. Chubukov, and A. G. Abanov, *Phys. Rev. B* **74**, 180403 (2006).